Journal of Physics: Conference Series **566** (2014) 012010 doi:10.1088/1742-6596/566/1/012010

Decoding the stellar fossils of the dusty Milky Way progenitors

M de Bennassuti[1,2], R Schneider[2], R Valiante[2] and S Salvadori[3]

[1] Dipartimento di Fisica, Sapienza, Università di Roma, Piazzale Aldo Moro 5, 00185 Roma, Italy
[2] INAF - Osservatorio Astronomico di Roma, Via di Frascati 33, 00040 Monte Porzio Catone, Italy
[3] Kapteyn Astronomical Institute, University of Groningen, Landleven 12, 9747 AD Groningen, The Netherlands

E-mail: matteo.debennassuti@oa-roma.inaf.it

Abstract. We investigate the metallicity distribution function (MDF) of the Galactic halo and the relative fraction of Carbon-normal and Carbon-rich stars using the semi-analytical code GAMETE. The code reconstructs the hierarchical merger tree of the Milky Way (MW) and follows the star formation history and the metal evolution in individual progenitors, including for the first time the formation and evolution of dust. We predict scaling relations between the dust, metal and gas masses for MW progenitors and compare them with observational data of galaxies at $0 \leq z < 6.3$. We find that the relative contribution of C-normal and C-enhanced stars to the MDF and its dependence on [Fe/H] allow to discriminate among different Pop III/II transition criteria as well as between different Initial Mass Functions (IMFs) and supernova (SN) yields for Population III stars.

1. Introduction

The physical conditions which enable the formation of the first low-mass and long-lived stars to form in the Universe is still a subject of debate. Numerical studies suggest the first Population III (Pop III) stars have masses mostly distributed between a few tens and a few hundred solar masses. The first supernovae (SNe) explode and seed the gas with metals and dust grains, changing the physical properties of star forming regions, eventually allowing the formation of the first low-mass Population II (Pop II) stars. Gas at low metallicity can achieve larger cooling rates through additional molecular species (HD, OH, CO, H_2O), fine structure line–cooling (mostly OI and CII) and thermal emission from dust grains. The relative importance of these coolants depends on the density (time) regime during the collapse and on the metal/dust content of the collapsing core.

The transition between Pop III and Pop II may be guided by different critical parameters: metallicity, $Z_{cr} = 10^{-3.8} Z_\odot$ [1], dust-to-gas mass ratio, $\mathcal{D}_{cr} \sim 4.4 \times 10^{-9}$ [2] or transition discriminant, $D_{trans,cr} = -3.5 \pm 0.2$ [3]. Most of the stars observed in the Galactic halo or in its dwarf satellites have $D_{trans} = \log_{10}(10^{[C/H]} + 0.9 \times 10^{[O/H]})$[1] $> D_{trans,cr}$, with the exception of SDSS J102915 [5]; this star provides a strong indication that low-mass star formation may have occurred in the absence of efficient metal-line cooling, supporting a dust-driven transition [6].

Hence, stellar archaeology of the most metal-poor stars is a promising way to constrain the environmental conditions for the formation of the first low-mass stars, exploring the star formation and the chemical enrichment of the Universe. In particular, the low-metallicity tail of the metallicity

[1] $[X/Y] = \log_{10}(N_X/N_Y) - \log_{10}(N_X/N_Y)_\odot$, for elements X and Y. Solar value are taken from [4].

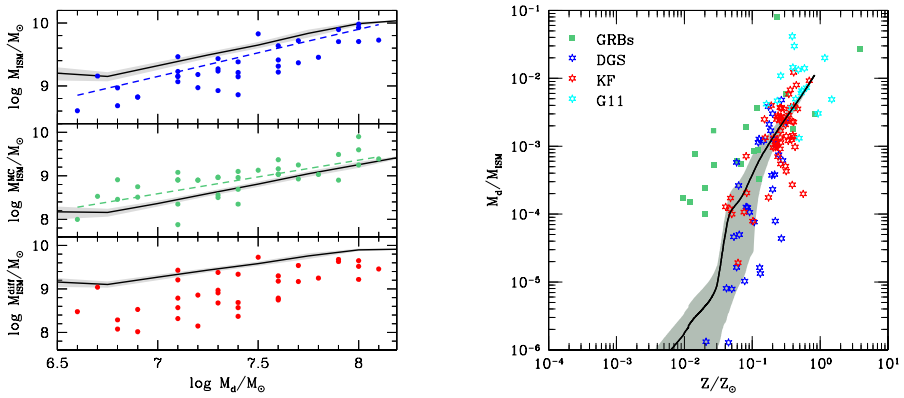

Figure 1. Comparison between the predicted properties of MW progenitors and observations. Solid lines represent averages over 50 independent merger histories of the MW and shaded regions the 1-σ dispersion. *Left panel*: correlation between the dust mass and the diffuse, molecular and total gas masses (from bottom to top). Observational data are taken from [7] with dashed lines indicating the best-fit linear relation for the data. *Right panel*: dust-to-gas mass ratio as a function of the gas metallicity. Stars refer to the sample analyzed by [8] and squares indicate the GRB data sample of [9].

distribution function (MDF, i.e. the number distribution of stars as a function of their [Fe/H]) at [Fe/H] < -2 and the observed surface elemental abundances of the most metal-poor stars can provide observational constraints on the nature of Pop III stars and on the formation efficiency of the first Pop II stars. Other hints are obtained by the so-called Carbon-enhanced extremely metal-poor stars (CEMP, with [C/Fe] $> +1$), whose fraction grows with decreasing [Fe/H] [10].

Here we describe an improved version of the hierarchical semi-analytical code GAlaxy MErger Tree and Evolution (GAMETE) [11]. Using this model, we predict the stellar, gas, metal and dust content of all the MW progenitors along the simulated merger trees, comparing our predictions with observations of the global properties of the MW and with the observed scaling relations inferred by different galaxy samples. We then apply the model to stellar archaeology to constrain the nature of the first stars.

2. Description of the model

The GAMETE code allows to reproduce the observed global properties of the MW, such as the mass of gas and stars, metallicity and dust-to-gas ratio, predicting their evolution along cosmic time. Enrichment processes are regulated by both Asymptotic Giant Branch (AGB) stars and SNe, which eject metals and dust into the ISM according to their stellar lifetime [12], accounting for partial dust destruction by the reverse shock in SN ejecta. We follow the formation and evolution of a MW-like galaxy in the framework of the Lambda Cold Dark Matter (ΛCDM) model using a binary Monte Carlo algorithm based on the Extended-Press and Schechter theory. The code traces the merger history backward in time, starting from a MW-like DM halo of $M_{MW} = 10^{12} M_\odot$ at redshift z = 0 up to z $\sim$ 20.

We have further improved GAMETE to describe the evolution of the gas in two separate phases of the ISM: a *diffuse* component (warm/hot low-density gas), where dust can be destroyed by SN shocks, and a *dense* or *molecular cloud* (MC) component (cold and dense gas), where star formation occurs and where dust grains can grow in mass by accreting gas-phase metals, being shielded from destructive processes.

Pop III stars are assumed to form with a Larson IMF (a power-law with an exponential cut-off below a characteristic mass, m_{ch}, chosen to have a $\sim 40\,M_\odot$ average mass [13]) either with masses in the range $[10-300]\,M_\odot$ or with masses in the range $[10-140]\,M_\odot$. Pop III stars enrich the ISM with metal and dust yields appropriate for core-collapse SNe [14, 15] or faint SNe [16] ($10\,M_\odot < m_* < 40\,M_\odot$) and PISNe [17, 18] ($140\,M_\odot < m_* < 260\,M_\odot$); outside these two mass ranges stars are assumed to directly collapse

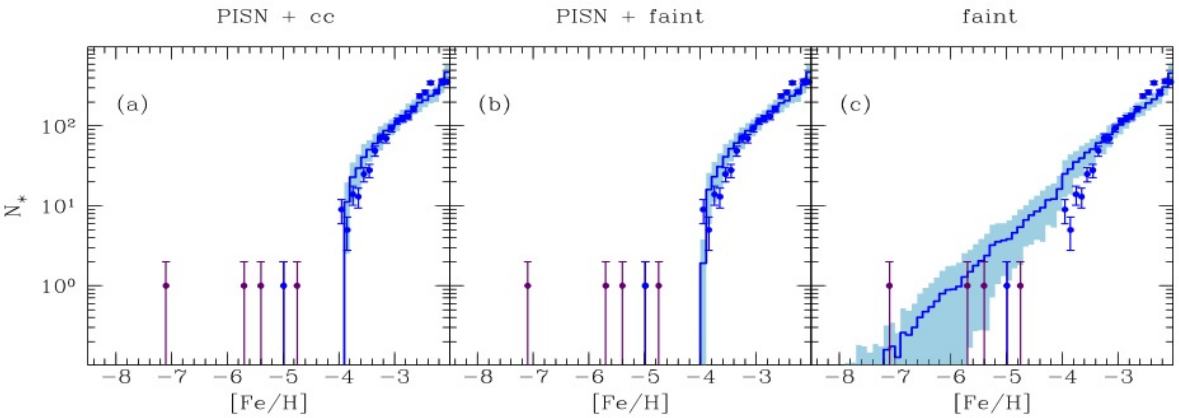

Figure 2. Simulated MDF as a function of [Fe/H] abundance. Solid lines show the results averaged over 50 merger trees with the shaded areas representing the 1-σ dispersion. The three panels are for: (*a*) PopIII IMF extending up to 300 $M_\odot$ with PISNe and core-collapse SN yields; (*b*) PopIII IMF up to 300 $M_\odot$ with PISNe and faint SNe yields; (*c*) PopIII IMF with stellar masses up to 140 $M_\odot$ and faint SNe yields only. Here we show the results obtained adopting the critical metallicity $Z_{cr} = 10^{-3.8} Z_\odot$ as transition criterium. Other criteria provide very similar results.

to black hole without ejecting the products of their nucleosynthesis. The main feature of faint SNe is the dramatically lower Fe yield ($\sim$ 5 orders of magnitude smaller with respect to ordinary core-collapse SNe).

Once the criterium for low-mass star formation is met (see Sec. 1), Pop II stars form according to a Larson IMF ([0.1 - 100] $M_\odot$, $m_{ch} = 0.35\ M_\odot$). Pop II yields account for both AGB [19, 20] and SNe [14, 15] contributions for stars with $m_* < 40\,M_\odot$.

The model free parameters are calibrated so as to reproduce the MW observations on the total mass of stars, the SFR and the mass of gas, dust and metals in the two ISM phases. Hereafter we refer to our fiducial model as the model where the Pop III/II transition occurs when $\mathcal{D} \geq \mathcal{D}_{cr} = 4.4 \times 10^{-9}$ and Pop III stars form in the range [10 − 140] $M_\odot$. All the details of this study are presented in [21].

3. Properties of the Milky Way progenitors

In this work we analyse the properties of the MW progenitors predicted by our reference model. By selecting the progenitors with stellar, dust and gas masses comparable to that of the observed sample of galaxies we have tested the predicted dust-to-metals and dust-to-gas scaling relations of our model.

In the left panel of Fig. 1 we compare the model predictions with local galaxies [7]. The behaviour of the simulated progenitors is globally consistent with observed data, with a slope close to the proposed linear regression (dashed lines). The correlation between the dust mass and total gas mass shows that MW progenitors are generally more gas-rich than typical galaxies in the observed sample, probably as a consequence of the earlier evolutionary stages of the model galaxies, which lie in the redshift range $0 < z < 4$. It is important to note that galaxies in the [7] sample have been classified to be HI-deficient, probably due to galaxy interactions in the cluster environment where they are embedded.

Additional constraints on the model can be obtained by comparing the predicted correlation between the dust-to-gas ratio and the gas metallicity. In the right panel of Fig. 1, we show the data points from three local galaxy surveys collected by [8] and the data collected by [9] over a wide redshift range $0.1 < z < 6.3$ using GRB afterglows. The observed data points indicate that the dust-to-gas ratio grows with the metallicity but with a large scatter, particularly at the lowest metallicities. A similar behaviour is found for the simulated MW progenitors.

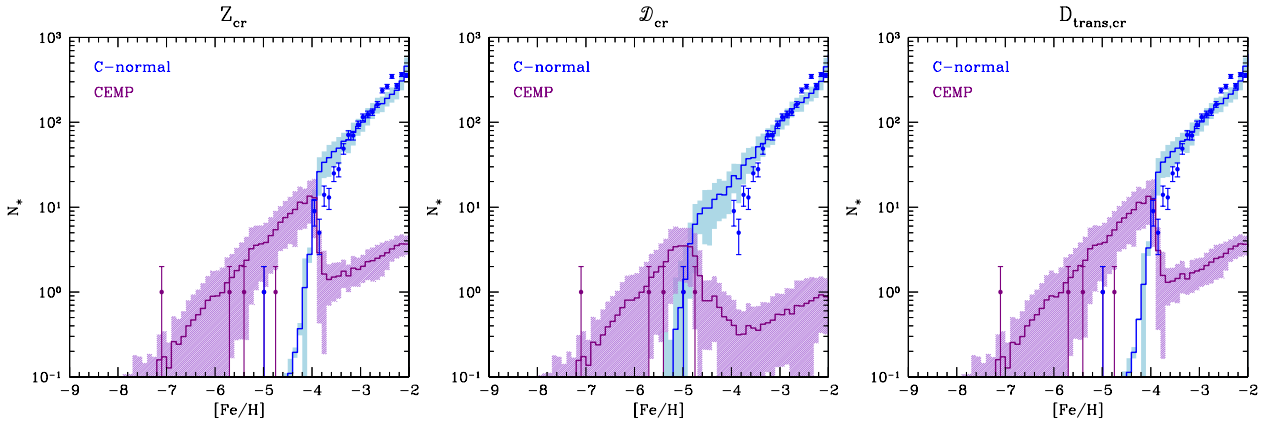

Figure 3. The contribution of C-enhanced stars ([C/Fe] $\geq$ 1.0, purple line and shaded region) and C-normal stars ([C/Fe] < 1, blue line and shaded region) to the theoretical MDF for different transition criteria (Z_{cr}, $\mathcal{D}_{cr}$, $D_{trans,cr}$, from left to right).

4. Stellar Archaeology

Here we study the predicted halo MDF for different Pop III mass ranges and/or Pop III SN yields, varying the criterium adopted for the Pop III/II transition.

Constraints on the Pop III IMF. Fig. 2 shows the comparison of models where the Pop III/II transition is driven by a critical metallicity of $Z_{cr} = 10^{-3.8} Z_{\odot}$. They differ only for the adopted Pop III IMF and corresponding yields, while the data points refer to the joint HK/HES sample that has already been used in [11]. We have added the 5 hyper-iron-poor stars currently known with [Fe/H] < −4.5.

The Pop III IMF, from left to right, extends up to (*a*) 300 $M_{\odot}$ (yields from cc-Sne and PISNe), (*b*) 300 $M_{\odot}$ (yields from faint SNe and PISNe) and (*c*) 140 $M_{\odot}$ (yields from faint SNe). In panels (*a*) and (*b*) it is evident that PISNe dominate the enrichment over cc and faint SNe, leading to the formation of stars with [Fe/H] $\gtrsim$ -4, at odds with observations. Panel (*c*) shows that if PISNe are excluded, then the iron enrichment is much slower, being dominated by faint SNe. As a result, the tail of the MDF extends to [Fe/H] $\sim$ -8, well into the observed range of the most iron-poor stars. The excess of predicted stars with −4.75 < [Fe/H] < −3.5 suggests that additional physical processes are at work, as radiative feedback effects that may prevent the gas in the first mini-halos from cooling, delaying or inhibiting star formation.

Constraints on the Pop III/II transition. For the same set of Pop III IMF and SN yields discussed above, the predicted MDF for different transition criteria are very similar to the Z_{cr} case: the mass range of PISN progenitors has to be excluded and faint SNe are needed to reproduce the low-metallicity tail of the MDF for all transition criteria, but the full MDF cannot discriminate between different transition criteria, being very similar in the three cases.

Tighter constraints on the Pop III/II transition can be set by separating the contribution to the MDF of C-normal and C-enhanced stars. The results are shown in Fig. 3. It is clear that CEMP stars dominate the low-[Fe/H] tail of the simulated MDF for all three cases. However, it is only in the case where Pop II stars from when $\mathcal{D} \geq \mathcal{D}_{crit}$, that the MDF of C-normal stars extends to [Fe/H] ~ -5.4, accounting for the observed data point that corresponds to SDSS J102915, the only C-normal star at these low-[Fe/H] currently known. Hence, the formation of SDSS J102915 must have followed alternative pathways, beyond that associated to fine-structure line cooling.

Carbon enhancement. Spectroscopic studies of metal poor stars have convincingly shown that the frequency of CEMP stars grows with decreasing [Fe/H] [10]. In Fig. 4 (right panel) we plot the observed fraction of CEMP stars (number of CEMP stars divided by the total number of stars) and of CEMP-no stars (CEMP stars which exhibit no over-abundances of the neutron-capture elements) for four different [Fe/H] bins. Empty squares refer to the fraction of CEMP stars and filled ones to the fraction of CEMP-no stars only, considering a subsample from [10], divided into CEMP-no and CEMP-r/s (CEMP stars

which exhibit elemental abundance patterns associated with *rapid* and/or *slow* process) stars following [22] (left panel). The simulated data underestimate the observations, even if the comparison must be restricted only to the CEMP-no fraction, since we do not consider mass-transfer effects in stellar binaries.

[23] have estimated that a fraction of dim SNe as large as 30%-50% is required to reconcile the observed SN rate with that predicted from the observed cosmic SFR. Assuming a similar fraction of Pop II faint-SNe we can better match the observed data points, as shown in Fig. 4.

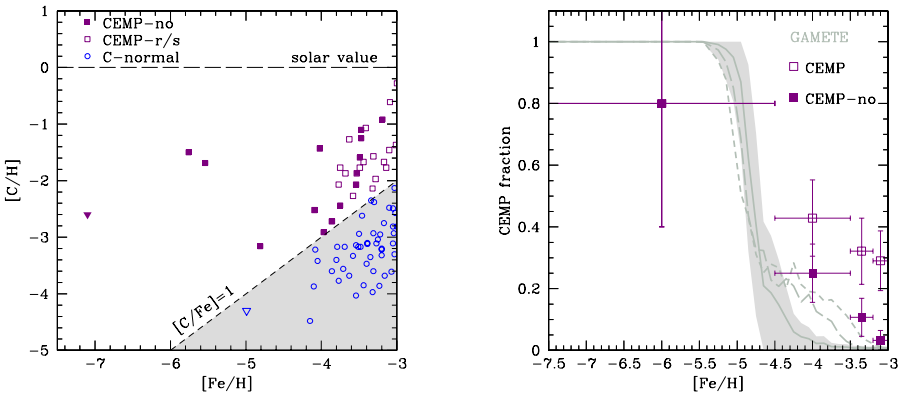

Figure 4. *Left panel:* C abundance as a function of [Fe/H] for the sample from [10, 22]. *Right panel:* observed fraction of CEMP (empty squares) and CEMP-no (filled squares) stars from [10, 22]. Errorbars are Poissonian errors (y-axis) and bin amplitude (x-axis). The grey solid line shows the predicted fraction of CEMP-no stars for the fiducial model averaged over 50 merger trees. The shaded region shows the 1-σ dispersion among different merger histories. The long-dashed and dashed lines show the results obtained when 30% and 50% of Pop II SN progenitors are assumed to explode as faint SNe, respectively.

5. Conclusions

We have presented an implemented version of the semi-analytical code GAMETE and a first applications of this new model to Stellar Archaeology. For the first time, we follow the star formation history and the enrichment in both metals and dust of the MW galaxy. Using a 2-phase description of the ISM we can follow the evolution of the atomic and molecular gas components and the separate evolution of metals and dust grains in these two phases. The model has been calibrated so as to reproduce the observed properties of the MW at z = 0 and we find that the simulated progenitors of the MW are in very good agreement with the scaling relations inferred from observations of local and GRB-host galaxies. When applied to Stellar Archaeology, the simulated MDF is very sensitive to the adopted Pop III IMF and metal yields. Current observations seem to require a largely sub-dominant contribution from PISNe to early metal enrichment, favouring Pop III stars with masses in the range $[10 - 140]M_{\odot}$ which explode as faint SNe. The analysis on the C abundance confirms the expectations that C-normal stars with [Fe/H] < -4.5, such as SDSS J102915, can form only assuming a dust driven transition.

Our fiducial model predicts a steeper decline of the CEMP fraction with [Fe/H] and an over-abundance of C-normal stars in the low-metallicity tail of the MDF compared to observations. This suggests that additional physical processes must be at play, most likely radiative feedback associated to the rising UV-background.

Acknowledgments

The research leading to these results has received funding from the European Research Council under the European Unions Seventh Framework Programme (FP/2007-2013) / ERC Grant Agreement n. 306476. This research was supported in part by the National Science Foundation under Grant No. NSF PHY11-25915. SS acknowledges support from Netherlands Organization for Scientific Research (NWO), VENI grant 639.041.233

References

[1] Bromm V, Ferrara A, Coppi P S and Larson R B 2001 *MNRAS* **328** 969
[2] Schneider R, Omukai K, Bianchi S and Valiante R 2012 *MNRAS* **419** 1566
[3] Frebel A and Norris J E 2013 *Planets, Stars and Stellar Systems* vol 5, ed T Oswalt and G Gilmore (Springer) chapter 3
[4] Caffau E, Ludwig H-G, Steffen M, Freytag B and Bonifacio P 2011a *Solar Phys.* **268** 255
[5] Caffau E *et al.* 2011b *Nature* **477** 67
[6] Schneider R, Valiante R, Ventura P, dell Agli F, Di Criscienzo M, Hirashita H and Kemper F. 2014 (arXiv:1404.7132)
[7] Corbelli E, Bianchi S, Cortese L, Giovanardi C, Magrini L, Pappalardo C, Boselli A and Bendo G J 2012 *A&A* **542** A32
[8] Rémy-Ruyer A *et al.* 2014 *A&A* **563** A31
[9] Zafar T and Watson D 2013 *A&A* **560** A26
[10] Yong D *et al.* 2013 *ApJ* **762** 26
[11] Salvadori S, Schneider R and Ferrara A 2007 *MNRAS* **381** 647
[12] Raiteri C M, Villata M and Navarro J F 1996 *A&A* **105** 315
[13] Hosokawa T and Omukai K 2009 *ApJ* **703** 1810
[14] Woosley S E and Weaver T A 1995 *ApJ* **101** 181
[15] Bianchi S and Schneider R 2007 *MNRAS* **378** 973
[16] Marassi S, Schneider R, Limongi M and Chieffi A 2014 *ApJ* **794** 100
[17] Heger A and Woosley S E 2002 *ApJ* **567** 532
[18] Schneider R, Ferrara A and Salvaterra R 2004 *MNRAS* **351** 1379
[19] Van den Hoek L B and Groenewegen M A T 1997 *A&A* **123** 305
[20] Zhukovska S, Gail H P and Trieloff M 2008 *A&A* **479** 453
[21] de Bennassuti M, Schneider R, Valiante R and Salvadori S 2014 *MNRAS* accepted
[22] Norris J E *et al.* 2013 *Apj* **762** 28
[23] Horiuchi S, Beacom J F, Kochanek C S, Prieto J L, Stanek K Z and Thompson T A 2011 *ApJ* **738** 154